Research Article

Modification of Functional Properties of Whey Protein Isolate Nanocomposite Films and Coatings with Nanoclays

Kerstin Müller,[1] Marius Jesdinszki,[1] and Markus Schmid[1,2]

[1]*Materials Development, Fraunhofer Institute for Process Engineering and Packaging IVV, Freising, Germany*
[2]*Chair for Food Packaging Technology, Technische Universität München, Freising, Germany*

Correspondence should be addressed to Markus Schmid; markus.schmid@ivv.fraunhofer.de

Whey protein based films have received considerable attention to be used for environment friendly packaging applications. However, such biopolymers are prevented for use in commercial packaging due to their limited mechanical and barrier performance. The addition of nanofillers is a common method to overcome those drawbacks of biopolymers. Whey protein isolate (WPI) based nanocomposite cast films and coatings were produced using montmorillonite and vermiculite clay as nanofiller in different concentrations. Uniform distribution of filler within the polymeric matrix was confirmed by scanning electron microscopy. Mechanical properties such as tensile strength as well as Young's modulus were increased after increasing the filler content, while elongation at break values decreased. All samples showed weak barrier potential against water vapor. Nanoclay incorporation, however, reduced water vapor transmission rates by approximately 50%. The oxygen barrier performance was improved for all nanocomposites. Results also indicated proportionality with the filler ratio according to applied models. The highest barrier improvement factors (BIF) were greater than five for the cast films and even greater than sixteen for the coatings. Developed WPI-based composites depicted nanoenhanced material properties representing a promising alternative to fossil-based packaging films.

1. Introduction

The ability of globular proteins such as whey proteins to form self-supporting films showed great potential for edible coatings or numerous packaging applications and have been widely studied [1–6]. However, applications are limited since without any modification, whey protein films only display a low moisture barrier as well as relatively poor mechanical properties compared to commercial and mainly fossil-based packaging materials [7–10]. Recently, polymer nanocomposites have received considerable attention in research and development [11–13] and are already widely used in areas such as automotive or packaging [12, 14]. Just like conventional microcomposites such as glass fiber enforced polymers, material stiffness can be increased by filler addition [15]. However, the nanosize scale brings several advantages such as a reinforcement in all directions, a less filler content needed (wt%), and a better surface finish [13]. In terms of barrier performance, the introduction of nanoclays or particles significantly influences the permeation behavior of

gases by extending diffusion path and time [13]. This effect can be specifically ascribed to exfoliated clay morphologies [16] based on the good platelets distribution within the matrix. Compared to conventional microcomposites, meaning composites with filler particles of approximately 60% vol in a microscale range, nanocomposites already show enhanced properties at low filler loads (<2% vol) [16]. In terms of nanocoatings, even super gas barrier coatings that match performance of metallized films have been developed [17]. Thus, the usage of nanometre-sized filler particles is also becoming a promising option to overcome the limited mechanical and barrier properties of biopolymer based films and coatings [7, 18]. Likewise, whey protein based nanocomposites have been a field of interest in the last decade [7, 11, 19–26] confirming this topic is of scientific and industrial relevance. In case of whey protein based films, present oxygen barrier properties could even potentially be further improved with nanoparticles. The main goal of this study was the development of exfoliated clay–whey protein nanocomposites with enhanced barrier and mechanical properties to maximize

material suitability for packaging applications in industrial applications. The related scientific issue was the effect of the nanofillers on the processability and functional properties of nanomodified whey protein isolate based cast films and coatings with emphasis on packaging related properties.

2. Material and Methods

2.1. Materials. Whey protein isolate (WPI) was obtained from Davisco Foods International Inc, USA. Glycerol was purchased by Chemsolute, Th. Geyer GmbH & Co KG, Germany. Deionized water was supplied by Fraunhofer IVV. The aqueous montmorillonite nanodispersions were provided by ITENE, Spain using Cloisite Na^+ and Nanofil 116 (both BYK Additives & Instruments, Wesel, Germany) with a clay concentration of 5% (w/w) for both dispersions. The Sunbar Vermiculite SX009 aqueous nanodispersion with a clay concentration of 7.6% (w/w) was obtained from SunChemical Ltd., UK. The chemically treated polyethylene terephthalate (PET) substrate Sarafil Polyplex Polyester Film with a thickness of 23 μm was supplied by Polyplex, Thailand.

2.2. Preparation of Film Forming Suspensions. Following the standard method by McHugh et al. [27] and Schmid et al. [4] a whey protein standard solution (WPSS) was produced. Therefore, 10% WPI (w/w) and deionized water are homogenized at room temperature in an electric stirrer (Thermomix 31-1, Vorwerk Deutschland Stiftung & Co. KG, Wuppertal, Germany) for 30 minutes at 200 rpm. Afterwards the solution is heated for 30 minutes at 90°C with continuous stirring (200 rpm). Thus, denaturation of the proteins was fully completed [28]. For cooling and degassing the solution is placed in an ultrasonic bath for 15 min (DT 514H, Ultrasonic peak output: 860 W, Bandelin electronic GmbH & Co. KG, Berlin, Germany) at 23°C and 37 kHz·s. After cooling down, glycerol (Glycerol, Merck KGaA, Darmstadt, Germany) is added to solution and stirred for further 30 minutes with the Thermomix at 200 rpm. Finally, the solution is placed in an ultrasonic bath again for degassing for further 15 minutes.

For the nanosuspensions, WPSS and the aqueous nanodispersions were mixed using a magnetic stirrer (Ikamag RCT, IKA-Labortechnik, Staufen, Germany) at 1200 rpm for at least one hour in different ratios to achieve the desired nanofiller ratios of 1%, 3%, 6%, and 9% (w/w) with reference to the protein content. To prevent agglomeration, it is highly important to gradually add the nanodispersion under continuous stirring. Additionally, the nanodispersions were redispersed for 30 minutes at 500 rpm electric stirrer (Thermomix 31-1, Vorwerk Deutschland Stiftung & Co. KG, Wuppertal, Germany) at room temperature and ultrasound treated with a sonotrode (Labsonic 1510, B. Braun, Melsungen, Germany) at 400 W for 45 minutes before mixing with WPSS.

2.3. Preparation of WPI/Clay Composite Cast Films and Coatings. All suspensions were coated on a chemically treated 23 μm PET film A4 sheets using the coating unit CUF 5 (Sumet Messtechnik, Denklingen, Germany) with 40 mm/s speed of application, a drying temperature of 105°C and a drying time of 5.5 minutes. For the target dry film thickness of 10 μm, a wired rod with 100 μm wet film thickness was used. Dried coatings were stored at ambient conditions of 23°C and 50% RH. Nanocomposite cast films were produced by solvent casting. Film forming suspensions were casted into square shaped Petri dishes with a target film thickness of 200 μm. Cast films were dried at ambient conditions of 23°C and 50% RH until they reach constant mass (approx. 8 days). All samples were stored at least 3 weeks prior to characterization in order to allow potential postcrosslinking to be completed [29].

2.4. Composite Film and Coating Characterization

2.4.1. Film Thickness. Thickness measurements were performed with a precision thickness gauge FT3 with 0.1 μm resolution (Rhopoint Instruments, Beyhill on Sea, United Kingdom) at five random positions around the film testing area and averaged for determination. For barrier and mechanical measurements, thicknesses were determined for each sample.

2.4.2. Mechanical Properties. Young's modulus (E), tensile strength (TS), and elongation at break (EB) of the cast films were tested using a tensile testing machine Z005 (Allround Line) of the Zwick GmbH & Co.KG, Ulm, Germany, at 23°C and 50% RH according to the DIN EN ISO 527-1. Tensile tests were performed with five strips of 15 mm width with a clamping length of 50 mm. The test speed was 50 mm/min with a load shut-off at 95% and a preload of 0.3 N.

2.4.3. Barrier Properties

Water Vapor Transmission Rate. The water vapor transmission rate was measured with a gravimetric method according to DIN 53122-1. The initial weight was measured by an analytical balance Mettler H315 of the Mettler-Toledo GmbH and the cups were then stored in a climate chamber of the Binder GmbH at 23°C and 85% RH. The samples were weighed four times in 48 hours until the weight gain stagnated. For each specimen, four replicates were tested. The water vapor transmission rate was calculated using the following formula [30]:

$$\text{WVTR} = \frac{24}{t} * \frac{\Delta m}{A} * 10^4 \ \left[g\,m^{-2}\,d^{-1} \right], \tag{1}$$

where t is time between two weight measurements of which Δm is calculated [h], Δm is weight difference of two successive weight measurements [g], and A is sample area [cm^2].

Oxygen Permeability. The oxygen permeability (OP) was measured with the oxygen-specific carrier gas method according to DIN 53380-3. The measurements were performed with a Mocon Ox-Tran Twin Oxygen Permeation Measuring Machine at a temperature of 23°C and 50% RH. The measurement stopped when a value was constant for at least ten hours. Two replicates of all coating and cast film specimens were determined.

For a better comparison of different polymers the permeability Q can be standardized to the Q_{100}–value relating to a

thickness of 100 μm [31]:

$$Q_{100} = Q * \frac{d}{100}. \tag{2}$$

To adapt permeability properties of a packaging material, multilayers can be used instead of raising the thickness of a monolayer. The total permeation of a multilayer system Q_{total} can be calculated as follows:

$$\frac{1}{Q_{total}} = \sum_{i=1}^{i=n} \frac{d_i}{P_i}. \tag{3}$$

2.4.4. Scanning Electron Microscopy (SEM). The scanning electron microscopy was performed with an ISI scanning electron microscope ABT 55 (ISI Akashi Beam Technology Corporation, Tokyo, Japan). Images were taken at 10 kV at different magnification and evaluated with a digital image scanning system DISS 5 by Point electronic GmbH, Halle (Saale), Germany. The measurements were performed in a high vacuum environment of 2×10^{-3} bar at room temperature. For sample preparation, cryofractures of selected samples were performed. The cross sections of the samples were fixed to the specimen holder with carbon tape and sputtered with a metal coating for improved conductivity.

2.5. Statistical Analysis. Statistical evaluations were performed using the computer programme Visual-XSel 12.0 Multivar (CRGRAPH, Munich, Germany). All measured data were tested on normal distribution. Depending on sample size, Kolmogorov-Smirnov test (sample size 3 or 4) or Anderson-Darling normality test (sample size $\geq$ 5) was used with a significance value α at 0.05. The Hampel test for outliers was used to detect and eliminate outliers of nonnormal distributed data with a significance value α at 0.05. Condition for elimination is that all other values are part of the same population, proved by normality tests. Comparison of sample sets was conducted with a multi-t-test using a significance value of 0.05.

2.6. Descriptive Statistics

2.6.1. Curve Fitting of the Modulus. According to literature, the models widely applied to describe the Young's moduli of composites filled with various types of filler are the Halpin-Tsai model and modified equations from it [12, 32]. According to this model, longitudinal elastic modulus can be expressed as follows:

$$\frac{E_c}{E_m} = \frac{1 + \xi\delta\phi}{1 - \delta\phi} \ [-], \tag{4}$$

where E_c is Young's modulus of the composite [MPa], E_m is Young's modulus of the matrix [MPa], and ϕ_f is volume fraction of the filler [—] with the constants ξ and δ given by

$$\delta = \frac{\left(E_f/E_m\right) - 1}{\left(E_f/E_m\right) + \xi} \ [-], \tag{5}$$

where E_f is Young's modulus of the filler [MPa] and E_m is Young's modulus of the matrix [MPa]

$$\xi = 2\left(\frac{l}{d}\right) = 2\alpha \ [-], \tag{6}$$

where l/d is the aspect ratio α of the reinforcing filler [12].

Since this model overestimated the experimental data, a Modulus Correction Factor (MCF) was introduced, adapting an approach by Wu and others [33]. Equation (7) describes the modified model used for calculations.

$$\frac{E_c}{E_m} = \frac{1 + (MCF)\,\xi\delta\phi}{1 - \delta\phi}. \tag{7}$$

The parameter MCF was determined for each type of used clay by minimizing the residual sum of squares RSS with Excel Solver (Microsoft Office Professional Plus, Version 14.0.7166.5000).

2.6.2. Predicting Barrier Properties. Table 1 shows different models that have been suggested to predict barrier properties of nanocomposites. The used models differ according to the particle geometry and calculations are based on aspect ratio α and the filler degree ϕ. Since only single particles are considered, those models assume fully exfoliated clays.
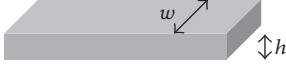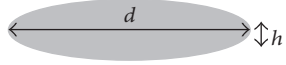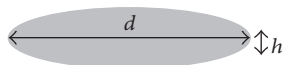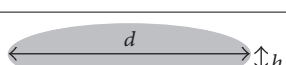
Considering the relatively simple model by Nielsen and making realistic assumptions with an aspect ratio of $\alpha = 500$ and a volume fraction of $\varphi = 0.07$ for nanocomposites, a barrier improvement of a factor of 20 is generally possible and was also already achieved in lab-scale experiments [39].

However, interactions between filler and matrix, state of exfoliation, and particle orientation also have to be taken into account. Therefore further important factors for the diffusion path extension are the state of dispersion, eventual aggregation or flocculation, and the orientation within the matrix [40]. The highest possible aspect ratio can be achieved by individual nanolayers requiring complete exfoliation [12]. Although best enhancement of barrier properties can be achieved with aligned platelets, the processing of exfoliated nanoclays mainly shows misaligned structures as well as nonexfoliated areas within the composites [12]. For those reasons, practical permeability data given by suppliers provide much lower barrier improvements compared to the theoretical values, normally with a factor of two [41].

3. Results and Discussion

3.1. Microstructure. The cross-sectional SEM images of selected WPI nanocomposite cast films and coatings can be seen in Figure 1. Nanoparticles are given in lighter color, while dark spots display small holes which are the traces of nanoparticles that remained on the opposite side of the cast films during hand fractioning. All composites show a homogeneous distribution of the nanofiller with maintaining WPI matrix structure. Even at the high nanoparticles concentrations only little agglomeration could be detected. The uniform distribution and dispersion of Cloisite Na$^+$ in the WPI matrix contributed to the mechanical and barrier

TABLE 1: Models for predicting barrier properties of platelet filled nanocomposites [13].

Model	Filler type	Particle geometry	Formulas	Reference
Nielsen	Ribbon[a]		$(P_0/P)(1 - \phi) = 1 + \alpha\phi/2$	[34]
Cussler (Random array)	Ribbon[a]		$(P_0/P)(1 - \phi) = \left(1 + \alpha\phi/3\right)^2$	[35]
Gusev and Lusti	Disk[b]		$(P_0/P)(1 - \phi) = \exp[(\alpha\phi/3.47)^{0.71}]$	[36]
Fredrickson and Bicerano	Disk[b]		$(P_0/P)(1 - \phi) = 4((1 + x + 0.1245x^2)/(2 + x))^2$ where $x = \alpha\phi/2\ln(\alpha/2)$	[37]
Bharadwaj	Disk[b]		$(P_0/P)(1 - \phi) = 1 + 0.667\alpha\phi(S + (1/2))$ where S = orientation factor (from $-1/2$ to 1)	[38]

[a]For ribbons, length is infinite, width, w; thickness, h; aspect ratio, $\alpha = w/h$; [b]for disks, circular shape of diameter d and thickness h; aspect ratio, $\alpha = d/h$.
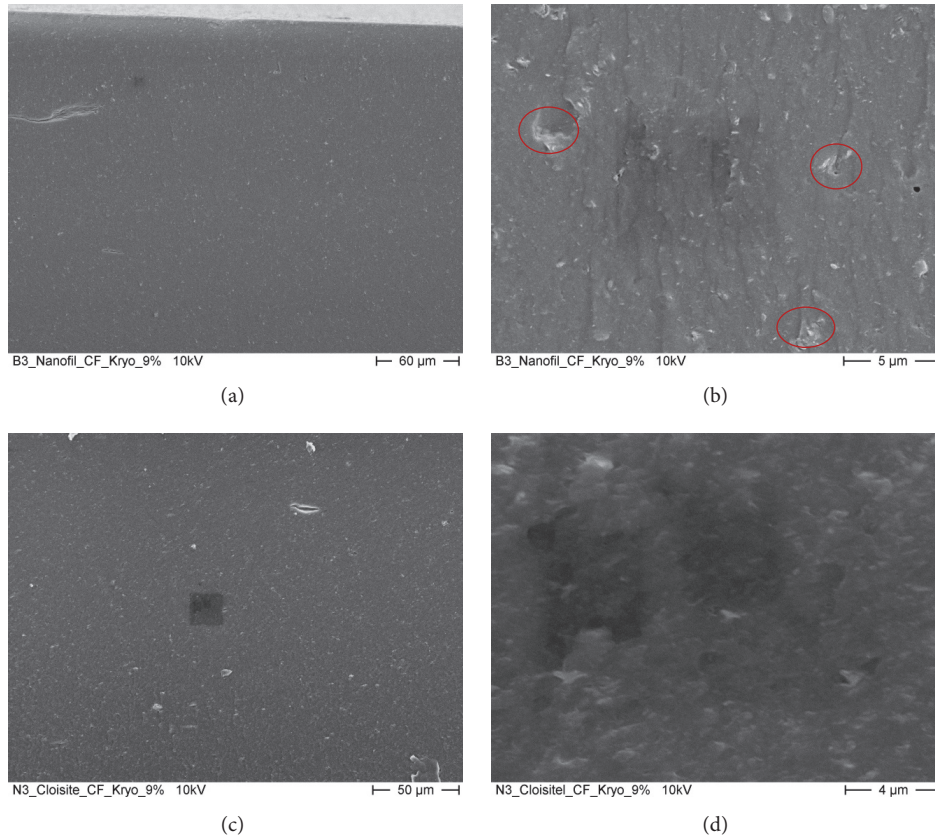

(a)

(b)

(c)

(d)

FIGURE 1: SEM images of selected nanomodified WPI-based cast films and coatings. Cryofractioned cross sections of 9% Nanofil cast films (a, b), 9% Cloisite Na$^+$ cast films (c, d) at different magnifications (scaling bottom right).

improvement of the nanocomposites. The poor improvements detected at the Nanofil composites could be due to the occurrence of comparably bigger agglomerates marked exemplary in Figure 1(b). Depending on the sample spot chosen for determination, distribution can of course differ.

3.2. Mechanical Properties. Measured data for mechanical properties of all casted nanocomposites can be seen in Table 2. All nanofillers used showed significant enhancement of Young's modulus and tensile strength at high nanoparticles concentrations. The increase of material stiffness and strength

TABLE 2: Mechanical data of WPI-based nanocomposites with different nanofillers. Columns with different letters are significantly different ($p \leq 0.05$) for each dataset compared to the zero sample.

Filler type	Filler ratio [wt%]	E [MPa]	TS [MPa]	EB [%]
—	0	58.54 ± 3.45[a]	3.69 ± 0.24[a]	135.48 ± 19.74[ab]
Cloisite Na$^+$	1	71.70 ± 3.85[b]	4.18 ± 0.23[b]	129.08 ± 17.48[ac]
	3	97.50 ± 4.44[c]	4.39 ± 0.14[b]	111.28 ± 1.54[cd]
	6	142.80 ± 3.11[d]	4.87 ± 0.09[c]	90.70 ± 26.69[de]
	9	208.40 ± 18.64[e]	5.67 ± 0.16[d]	64.26 ± 14.39[e]
Nanofil 116	1	57.12 ± 12.27[a]	4.07 ± 0.13[b]	136.78 ± 13.07[a]
	3	78.36 ± 4.28[b]	4.37 ± 0.17[c]	141.04 ± 15.13[a]
	6	80.32 ± 16.48[b]	4.90 ± 0.15[d]	144.30 ± 5.07[a]
	9	123.00 ± 6.52[c]	5.28 ± 0.26[e]	116.90 ± 12.96[b]
Sunbar	1	77.78 ± 15.27[b]	3.95 ± 0.40[a]	125.54 ± 20.13[a]
	3	121.46 ± 21.90[c]	4.10 ± 0.19[b]	69.50 ± 10.79[c]
	6	218.25 ± 5.12[d]	4.76 ± 0.58[b]	29.72 ± 3.15[d]
	9	283.40 ± 35.98[e]	6.19 ± 0.10[c]	21.96 ± 1.53[e]

by the incorporation of nanofillers into whey protein based matrices was also confirmed by several studies [7, 21, 24–26]. Similar to the modulus, the material reinforcement and therewith higher strength levels depend on composite morphology, since better exfoliation leads to higher improvements. However, tensile strength as well as elongation at break are nonlinear mechanical properties and decrease beyond a critical filler ratio [12]. Here, the transfer of load between filler and matrix is decisive and depends on their compatibility. Results indicate efficient interfacial interaction between matrix and filler at all nanoclays used. In terms of tensile strength, measured improvements are comparable to other studies using nanoclay in whey protein based matrices [21, 24–26]. Furthermore, the continuous increase in tensile strength values is another evidence for a good distribution of the nanofiller at all concentrations as well as good interface adhesion.

Since the addition of filler into a polymeric matrix decreases material ductility, elongation levels of nanocomposites are typically lower than those of the polymer itself [13]. As discussed before, the incorporation of nanofiller contributes to a reinforcement of the cast films and reduces their flexibility at the same time [42], which explains a general decrease of elongation at break with increasing nanofiller ratio at the measured samples. Except for the highest concentration, elongations at break of the Nanofil composites were not statistically different to pure WPSS cast films ($p >$ 0.05) and also did not contribute to mechanical strength as good as the other fillers used. The diverse results of the different clays used can be attributed to different matrix-filler interactions, inhomogeneous spots at the measured samples, or the differences in sample thicknesses. Comparable studies using nanofillers in protein based matrices also showed diverse results. Wakai and others also incorporated 5% ((w/w), relative to the protein content) MMT clay into WPI matrix leading to a comparable decrease in elongation at break by 34% [43], while Sothornvit and others reported no significant differences at 5% Nanofiller (Cloisite Na$^+$)

in MMT/WPI cast films [20] which was explained by the assumption of incomplete nanoclay dispersion.

As expected by composite theory, the modulus was increased when a filler was incorporated into the polymeric matrix. Young's modulus is a linear mechanical property which is measured at low strains and reflects material stiffness [44]. In the case of polymer nanocomposites, stiffness generally increases with the volume fraction of the nanofiller, as long as sufficient dispersion and exfoliation are ensured [12].

To be able to predict the Young's modulus of such nanocomposites, the data was also fitted to the described modified Halpin-Tsai model. Therefore, the Young's modulus of the Cloisite Na$^+$ and Nanofil 116 fillers was assumed to be at 178 GPa, following an estimation by Fornes and Paul for MMT clay [45]. There was no explicit modulus data found for vermiculite clays. Since the range for Young's moduli of layered silica lies between 178 and 265 GPa [45–47], a realistic assumption of 200 GPa was made for the Sunbar vermiculite filler. The modification of the Halpin-Tsai model was needed due to overestimation of the experimental data. This is because the Halpin-Tsai model is based on assumptions that are only partly fulfilled by the examined nanocomposites. The model presumes linear elastic and isotropic matrix and filler as well as completely oriented particles of similar size and shape. Additionally, the properties of matrix and filler do not change in the presence of each other [48]. Also, occurring agglomeration and the state of exfoliation are not considered. The MCF takes deviations into account and gives a better model fit. Table 3 shows the used and calculated constants and parameters for the curve fitting.

The determined Young's modulus values ranged from approximately 60 to 180 MPa. Therefore, the RSS values also lie in a three-digit range. As described before, Sunbar and Cloisite Na$^+$ samples showed proportionality between filler ratio and Young's modulus according to the Halpin-Tsai model. RSS as well as R^2 indicates a good model fit; therefore it is possible to describe this proportionality with the adapted Halpin-Tsai model. The correction factors of

TABLE 3: Modified Halpin-Tsai Parameters for different fillers used in whey protein nanocomposites.

Filler type	ξ	δ	MCF	RSS [MPa^2]	R^2
Cloisite Na$^+$	140	0.9557	0.2461	103.727	0.9432
Nanofil 116	140	0.9557	0.0893	315.128	0.5275
Sunbar	200	0.9444	0.2334	271.132	0.7058

Cloisite Na$^+$ and Sunbar filler lie in the same range. As can be seen in Figure 2, for the Nanofil filler, the initial Halpin-Tsai theory highly overestimated Young's modulus leading to a lower MCF. This is also in line with the varying results at other tested mechanical properties indicating a heterogeneous filler distribution and occurring agglomeration. Furthermore, inherent moisture of the Nanofil clay is lower compared to the Cloisite clay, resulting in an actual lower net volume of the silicate filler. Therefore also lower R^2 and higher RSS values were determined.

3.3. Barrier Properties Oxygen Permeability

3.3.1. Coatings. To evaluate oxygen barrier properties of the coatings, permeabilities for the coated monolayer without the PET substrate were calculated by converting (3) with the values measured for the bilayer-system and the pure substrate. Coating thicknesses varied from approximately 7 to 9 μm; therefore resulting values were additionally normalized to 100 μm thickness following formula (2). Cloisite Na$^+$ as well as the Sunbar filler both showed decreases at each concentration step, indicating proportionality between filler ratio and permeability (see Figure 3). The lowest permeability of 2.097 [(cm^3 100 μm)/(m^2 d bar)] was determined for a monolayer with 9% ((w/w), relative to protein) Sunbar filler. The corresponding BIF, defined as the ratio of the permeability through the pure whey protein film and the permeability through the respective composite, was higher than 16. Weizman et al. [49] also used MMT clay for whey protein isolate based coatings with comparable OP for the zero sample. However, compared to Cloisite Na$^+$, barrier improvements at measured 1% and 5% clay were lower (appr. 30 and 25 (cm^3 100 μm)/(m^2 d bar), resp.) compared to this study.

3.3.2. Cast Films. To get comparable results and since cast film thicknesses of the samples varied, measured values were normalized to 100 μm thickness (2).

All samples showed improved barrier performance with the addition of nanofiller, which can be seen in Figure 4. The WPSS sample gave an OP of approx.. 80 cm^3/(m^2 d bar) for 100 μm film thickness. By adding Closite Na$^+$, oxygen permeabilities were reduced up to a factor two at the highest filler ratio of 9% (w/w). The Sunbar Vermiculite filler gave even better results with barrier improvements of 20, 50, 75, and even 80% for the respective ratios compared to the zero sample. Measured values for the Nanofil sample set varied widely and showed no expected decrease of OP with increasing filler ratio. Explanation could be given by filler agglomeration at the measured sample spots generating no
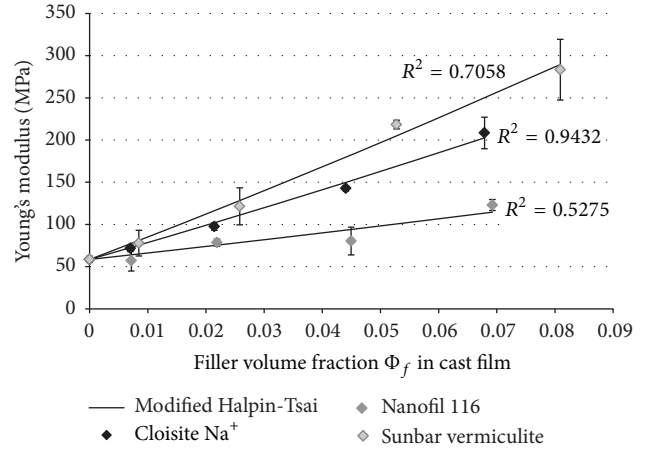

FIGURE 2: Experimental and theoretical Young's modulus of whey protein nanocomposite cast films reinforced with different fillers plotted as a function of their volume fraction with theoretical data given by a modified Halpin-Tsai model.
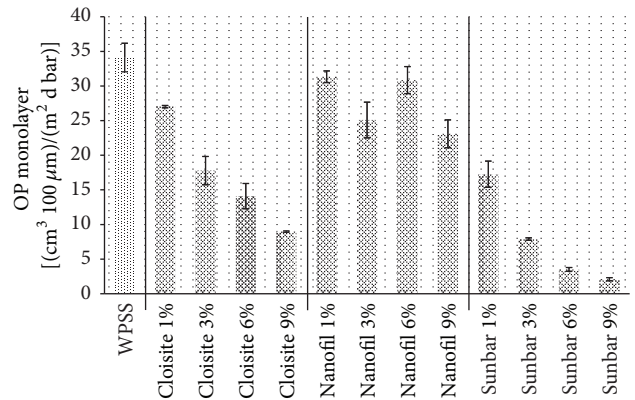

FIGURE 3: Influence of filler ratio on OP of whey protein nanocomposite coated monolayer with different nanofillers. Values were normalized to 100 μm thickness. Error bars show minimum and maximum value (twofold determination).

tortuous pathway for the permeating oxygen molecules. Furthermore, Nanofil 116 clays depict higher inherent moisture (8–13%) compared to the similar MMT clay Cloisite Na$^+$ (4–9%). Therefore, the net volume of silicate layers in the composite is lower which could explain lower effects that also were observed at mechanical measurements. In terms of barrier properties and especially oxygen permeability, inherent moisture of the Nanofil clay could have had a negative effect on the barrier performance, since oxygen permeability of whey protein based films is a moisture-related property with decreasing barrier performance at increasing moisture [50]. Similar observations were also made for water vapor measurements, confirming this declaration.

Since both the Cloisite Na$^+$ and the Sunbar Vermiculite sample sets showed expected decreases with increasing filler content, measured data was compared to the usual applied models for predicting the barrier performance of polymer
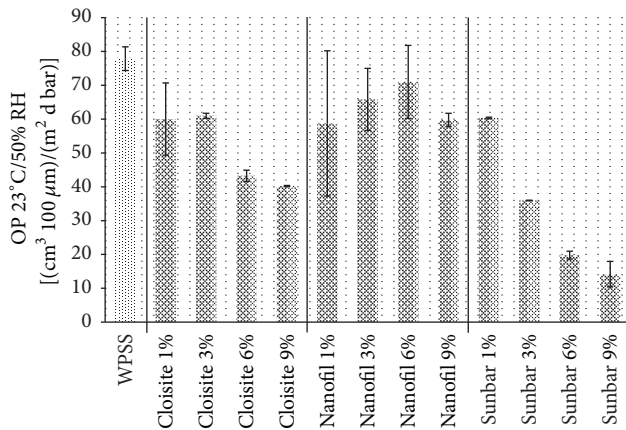
FIGURE 4: Influence of filler ratio on OP of whey protein nanocomposite cast films with different nanofillers. Error bars show minimum and maximum value (twofold determination).
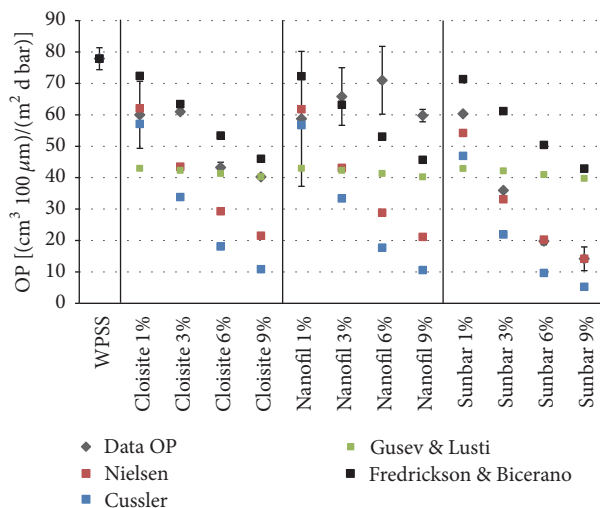

FIGURE 5: Comparison of OP original data with results from various models for predicting barrier properties of platelet filled nanocomposites.
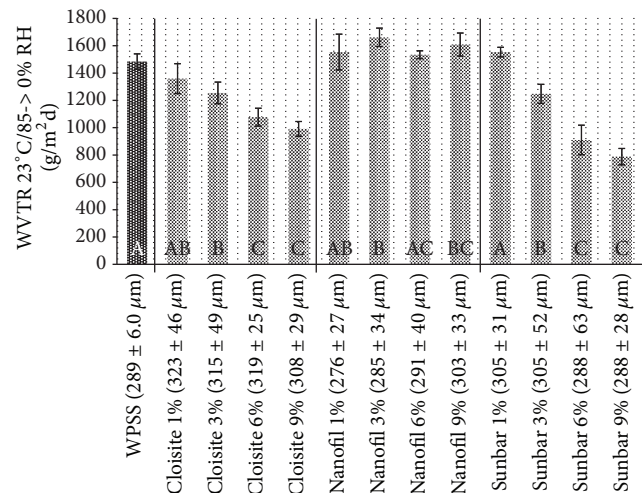

FIGURE 6: Influence of filler ratio on water vapor transmission rates of nano whey protein composite cast films with different nanofillers. Average thicknesses of each sample set after measurement are given in parentheses after the sample labeling. Columns with different letters are significantly different ($p \leq 0.05$) for each dataset compared to the zero sample (WPSS).

compared to MMT, exfoliation processes are favoured in vermiculite clay. Additionally, due to different densities, the net volume ratio of platelets is higher with vermiculite clay. In terms of oxygen permeability, especially a higher state of exfoliation could have caused higher decreases and an approximation to the simple expression by Nielsen. All other models showed higher variations and mainly overestimated the measured data and are therefore not applicable for the used matrix-filler combination. However, for a suitable prediction of oxygen barrier properties for such WPI-based nanocomposites, the type of clay as well as the state of exfoliation and dispersion should be considered. Therefore, further parameters should be included to modify existing models if a barrier performance prediction is desired.

3.4. Water Vapor Permeability. Figure 6 shows water vapor transmission rates of all denatured specimen (cast films). All samples only showed weak barrier potential against water vapor. However, using Cloisite Na$^+$ and Sunbar Vermiculite as filler, WVTR could be significantly reduced ($p \leq 0.05$) by approximately 30 and 50% at the highest filler ratio.

The slight increase in WVTR when adding nanofillers (Nanofil and Sunbar) to the cast films could be explained by a decreased post-cross-linking of the WPI matrix due to the presence of the nanoplatelets/clays. At higher concentrations, the influence of an extended tortuous pathway for water vapor molecules takes more account and WVTR is decreased with increasing filler ratio at both the Cloisite and Sunbar filler. Nanofil specimen did not contribute to water vapor barrier capacities of WPI cast films. Possible reasons could be agglomeration of the nanofiller, so that no tortuous pathway was generated. Additionally, sample swelling could have caused free volume and easy water vapor solubility within the

nanocomposites. The following figure shows the measured data and the corresponding theoretical values for four different models. The aspect ratio for Cloisite Na$^+$ of 70 was already applied in a former study [43], for both other fillers realistic values were assumed with 70 for Nanofil 116 (also MMT clay) and 100 for Sunbar Vermiculite based on found results, since there was no information available.

For the Cloisite Na$^+$ filler, the model by Fredrickson and Bicerano seemed most appropriate to predict barrier properties based on visual assessment (see Figure 5). Unlike Nielsen or Cussler, Fredrickson and Bicerano assumed disk-shaped platelets that are aligned, but positionally disordered [37], which is presumed to be present in here produced nanocomposites. Sunbar Vermiculite showed higher decreases and lowest deviations to the simple model by Nielsen. Due to a higher basal spacing and inherent water
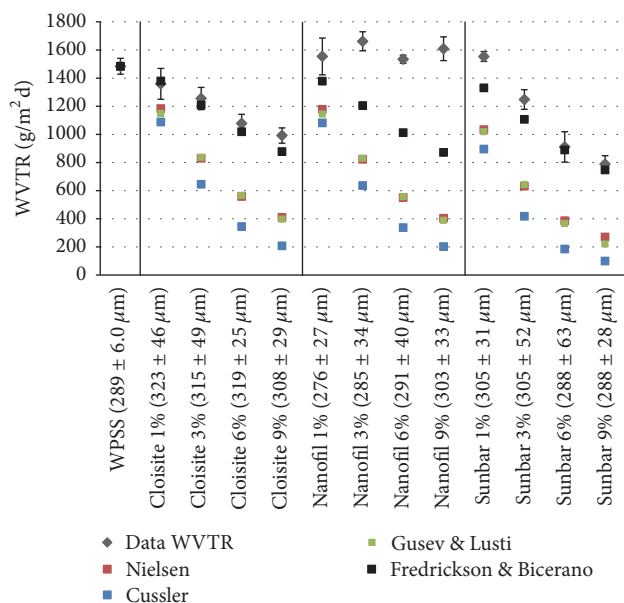
FIGURE 7: Comparison of WVTR original data with results from various models for predicting barrier properties of platelet filled nanocomposites. Average thicknesses of each sample set after measurement are given in parentheses after the sample labeling.

matrix so that even higher transmission rates were detected. Permeation tests performed at large relative humidity steps unluckily lead to swelling of WPI films. Theoretical constant diffusivity and constant thickness cannot not be assumed anymore, resulting in inaccurate measurement values [22]. Compared to a study by Sothornvit et al. [20] also using Cloisite Na$^+$ clay (5% w/w relative to protein) in whey protein isolate/clay nanocomposites, measured WVTR values were much higher. However, the improvement by clay incorporation is of the same order of magnitude. Similar to the OP data, WVTR values were compared to common models for barrier predictions (see Figure 7).

Cloisite Na$^+$ and Sunbar Vermiculite filler showed good model adjustment for barrier prediction. At WVTR measurements, the Fredrickson and Bicerano gave the best model fit by visual assessment for both sample sets. All other models displayed high differences between measured data and theoretic calculated values.

Compared to the oxygen permeation values, much lower barrier improvements were achieved with the same nanocomposite system. On the one hand, these results can clearly be attributed to the sample swelling which appeared at water vapor transmission measurements. On the other hand, however, other studies using nanoclay fillers in nonswelling PET matrix also revealed oxygen barrier improvements but no significant improvements concerning the water vapor transmission [51]. This different behavior of oxygen and water vapor transmission within the same system can be ascribed to occurring interactions between the permeating molecules with each other, the polymer matrix or the filler. Water vapor molecules generally have a greater tendency to those interactions by forming hydrogen bonds, making

barrier improvements rather a function of hydrophobicity of the filler surface [12]. Since the used nanofillers rather display hydrophilic properties, stronger interactions between water vapor molecules and the filler platelets can occur resulting in lower barrier performances compared to oxygen. Existing models do not take interaction between filler and matrix into account. Thus, at least for water vapor permeability in protein based nanocomposites, interaction parameters should be established and used to adapt models for barrier predictions.

4. Conclusions

The homogeneous distribution proved by microscopy techniques indicated good compatibility and strong interactions between filler and matrix and confirmed a suitable method for the described processing of WPI-based nanocomposites. This was also reflected by the results of the mechanical and barrier properties characterizations. The incorporation of nanofillers gave improved stiffness and strength to the composite materials. Since no decline was visible at elongation and tensile strength measurements, the limit for nonlinear mechanical properties, meaning a critical filler ratio, is not reached yet; therefore further material reinforcement can be expected with higher filler ratios. Just like other protein based films, samples only showed weak barrier potential against water vapor. However, a significant WVTR reduction of approximately 50% was achieved using 9% (w/w) Sunbar Vermiculite as filler in cast films. For all prepared nanocomposites, oxygen barrier improvements were achieved. The highest BIF above 16 was achieved for the 9% (w/w) Sunbar Vermiculite nanocomposite coating with a permeability comparable to conventionally used oxygen barrier materials. Therefore, the development of WPI-based nanocomposites could expand the potential of whey proteins coating to be used in sustainable and biodegradable packaging solutions. Due to shown mechanical and barrier improvements, such nanocomposites could present an alternative to fossil-based packaging materials.

Conflicts of Interest

The authors declare that there are no conflicts of interest regarding the publication of this paper.
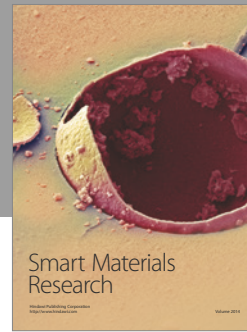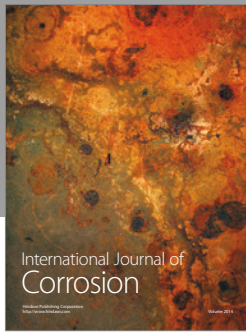
Acknowledgments

References

[1] T. Lefèvre, M. Subirade, and M. Pézolet, "Molecular description of the formation and structure of plasticized globular protein films," *Biomacromolecules*, vol. 6, no. 6, pp. 3209–3219, 2005.

[2] D. Plackett, "Biopolymers - New Materials for Sustainable Films and Coatings," *Biopolymers - New Materials for Sustainable Films and Coatings*, 2011.

[3] P. S. P. De Herrmann, C. M. Pedroso Yoshida, A. J. Antunes, and J. A. Marcondes, "Surface evaluation of whey protein films by atomic force microscopy and water vapour permeability analysis," *Packaging Technology and Science*, vol. 17, no. 5, pp. 267–273, 2004.

[4] M. Schmid, K. Dallmann, and E. Bugnicourt, "Properties of whey-protein-coated films and laminates as novel recyclable food packaging materials with excellent barrier properties," *International Journal of Polymer Science*, vol. 2012, Article ID 562381, 7 pages, 2012.

[5] F. Hammann and M. Schmid, "Determination and quantification of molecular interactions in protein films: a review," *Materials*, vol. 7, no. 12, pp. 7975–7996, 2014.

[6] J. Zink, T. Wyrobnik, T. Prinz, and M. Schmid, "Physical, chemical and biochemical modifications of protein-based films and coatings: an extensive review," *International Journal of Molecular Sciences*, vol. 17, no. 9, p. 1376, 2016.

[7] J. J. Zhou, S. Y. Wang, and S. Gunasekaran, "Preparation and characterization of whey protein film incorporated with TiO2 nanoparticles," *Journal of Food Science*, vol. 74, no. 7, pp. N50–N56, 2009.

[8] M. B. Pérez-Gago, P. Nadaud, and J. M. Krochta, "Water vapor permeability, solubility, and tensile properties of heat-denatured versus native whey protein films," *Journal of Food Science*, vol. 64, no. 6, pp. 1034–1037, 1999.

[9] L. Cisneros-Zevallos and J. M. Krochta, "Whey protein coatings for fresh fruits and relative humidity effects," *Journal of Food Science*, vol. 68, no. 1, pp. 176–181, 2003.

[10] B. Ouattara, L. T. Canh, C. Vachon, M. A. Mateescu, and M. Lacroix, "Use of γ-irradiation cross-linking to improve the water vapor permeability and the chemical stability of milk protein films," *Radiation Physics and Chemistry*, vol. 63, no. 3-6, pp. 821–825, 2002.

[11] M. S. Hedenqvist, A. Backman, M. Gällstedt, R. H. Boyd, and U. W. Gedde, "Morphology and diffusion properties of whey/montmorillonite nanocomposites," *Composites Science and Technology*, vol. 66, no. 13, pp. 2350–2359, 2006.

[12] V. Mittal, *Optimization of polymer nanocomposite properties*, John Wiley and Sons, 2009.

[13] D. R. Paul and L. M. Robeson, "Polymer nanotechnology: nanocomposites," *Polymer*, vol. 49, no. 15, pp. 3187–3204, 2008.

[14] K. Müller, E. Bugnicourt, M. Latorre et al. et al., "Review on the processing and properties of polymer nanocomposites and nanocoatings and their applications in the packaging, automotive and solar energy fields," *Nanomaterials*, vol. 7, p. 74, 2017.

[15] T. G. Gopakumar, J. A. Lee, M. Kontopoulou, and J. S. Parent, "Influence of clay exfoliation on the physical properties of montmorillonite/polyethylene composites," *Polymer*, vol. 43, no. 20, pp. 5483–5491, 2002.

[16] A. Arora and G. W. Padua, "Review: nanocomposites in food packaging," *Journal of Food Science*, vol. 75, no. 1, pp. R43–R49, 2010.

[17] K. M. Holder, B. R. Spears, M. E. Huff, M. A. Priolo, E. Harth, and J. C. Grunlan, "Stretchable gas barrier achieved with partially hydrogen-bonded multilayer nanocoating," *Macromolecular Rapid Communications*, vol. 35, no. 10, pp. 960–964, 2014.

[18] M. Avella, J. J. De Vlieger, M. E. Errico, S. Fischer, P. Vacca, and M. G. Volpe, "Biodegradable starch/clay nanocomposite films for food packaging applications," *Food Chemistry*, vol. 93, no. 3, pp. 467–474, 2005.

[19] R. Sothornvit, S.-I. Hong, D. J. An, and J.-W. Rhim, "Effect of clay content on the physical and antimicrobial properties of whey protein isolate/organo-clay composite films," *LWT - Food Science and Technology*, vol. 43, no. 2, pp. 279–284, 2010.

[20] R. Sothornvit, J.-W. Rhim, and S.-I. Hong, "Effect of nano-clay type on the physical and antimicrobial properties of whey protein isolate/clay composite films," *Journal of Food Engineering*, vol. 91, no. 3, pp. 468–473, 2009.

[21] M. Hassannia-Kolaee, F. Khodaiyan, R. Pourahmad, and I. Shahabi-Ghafarrokhi, "Development of ecofriendly bionanocomposite: Whey protein isolate/pullulan films with nano-SiO2," *International Journal of Biological Macromolecules*, vol. 86, pp. 139–144, 2016.

[22] P. Oymaci and S. A. Altinkaya, "Improvement of barrier and mechanical properties of whey protein isolate based food packaging films by incorporation of zein nanoparticles as a novel bionanocomposite," *Food Hydrocolloids*, vol. 54, pp. 1–9, 2016.

[23] Y. Li, Y. Jiang, F. Liu, F. Ren, G. Zhao, and X. Leng, "Fabrication and characterization of TiO2/whey protein isolate nanocomposite film," *Food Hydrocolloids*, vol. 25, no. 5, pp. 1098–1104, 2011.

[24] V. M. Azevedo, M. V. Dias, S. V. Borges et al., "Development of whey protein isolate bio-nanocomposites: Effect of montmorillonite and citric acid on structural, thermal, morphological and mechanical properties," *Food Hydrocolloids*, vol. 48, pp. 179–188, 2015.

[25] M. Hassannia-Kolaee, F. Khodaiyan, and I. Shahabi-Ghafarrokhi, "Modification of functional properties of pullulan–whey protein bionanocomposite films with nanoclay," *Journal of Food Science and Technology*, vol. 53, no. 2, pp. 1294–1302, 2016.

[26] M. Zolfi, F. Khodaiyan, M. Mousavi, and M. Hashemi, "The improvement of characteristics of biodegradable films made from kefiran-whey protein by nanoparticle incorporation," *Carbohydrate Polymers*, vol. 109, pp. 118–125, 2014.

[27] T. H. McHugh, J. F. Aujard, and J. M. Krochta, "Plasticized whey-protein edible films: water-vapor permeability properties," *Journal of Food Science*, vol. 59, no. 2, pp. 416–419, 1994.

[28] M. Schmid, B. Krimmel, U. Grupa, and K. Noller, "Effects of thermally induced denaturation on technological-functional properties of whey protein isolate based films," *Journal of Dairy Science*, vol. 97, no. 9, pp. 5315–5327, 2014.

[29] M. Schmid, K. Reichert, F. Hammann, and A. Stäbler, "Storage time-dependent alteration of molecular interaction–property

relationships of whey protein isolate-based films and coatings," *Journal of Materials Science*, vol. 50, no. 12, pp. 4396–4404, 2015.

[30] DIN, "Bestimmung der wasserdampfdurchlässigkeit. Teil 1: Gravimetrisches verfahren," in *DIN 53122-1, e.V., D.I.f.N., Ed. Deutsches Institut für Normung*, 2001.

[31] G. Menges, *Werkstoffkunde kunststoffe*, Hanser Fachbuchverlag, 2002.

[32] E. Esmizadeh, G. Naderi, and M. H. R. Ghoreishy, "Modification of Theoretical models to predict mechanical behavior of PVC/NBR/organoclay nanocomposites," *Journal of Applied Polymer Science*, vol. 130, no. 5, pp. 3229–3239, 2013.

[33] Y.-P. Wu, Q.-X. Jia, D.-S. Yu, and L.-Q. Zhang, "Modeling Young's modulus of rubber-clay nanocomposites using composite theories," *Polymer Testing*, vol. 23, no. 8, pp. 903–909, 2004.

[34] L. E. Nielsen, "Models for the Permeability of Filled Polymer Systems," *Journal of Macromolecular Science: Part A - Chemistry*, vol. 1, no. 5, pp. 929–942, 1967.

[35] N. K. Lape, E. E. Nuxoll, and E. L. Cussler, "Polydisperse flakes in barrier films," *Journal of Membrane Science*, vol. 236, no. 1-2, pp. 29–37, 2004.

[36] A. A. Gusev and H. R. Lusti, "Rational design of nanocomposites for barrier applications," *Advanced Materials*, vol. 13, no. 21, pp. 1641–1643, 2001.

[37] G. H. Fredrickson and J. Bicerano, "Barrier properties of oriented disk composites," *The Journal of chemical physics*, vol. 110, pp. 2181–2188, 1999.

[38] R. K. Bharadwaj, "Modeling the barrier properties of polymer-layered silicate nanocomposites," *Macromolecules*, vol. 34, no. 26, pp. 9189–9192, 2001.

[39] K. Müller, "Multilayer films for bag-in-container systems used in disposable kegs: Basic principles of possible barrier concepts," *Brewing Science*, vol. 66, pp. 31–36, 2013.

[40] V. Rastogi and P. Samyn, "Bio-based coatings for paper applications," *Coatings*, vol. 5, p. 887, 2015.

[41] H.-C. Langowski, "Permeation of gases and condensable substances through monolayer and multilayer structures," in *Plastic Packaging*, pp. 297–347, Wiley-VCH Verlag GmbH & Co, 2008.

[42] J.-W. Rhim, "Effect of clay contents on mechanical and water vapor barrier properties of agar-based nanocomposite films," *Carbohydrate Polymers*, vol. 86, no. 2, pp. 691–699, 2011.

[43] M. Wakai and E. Almenar, "Effect of the presence of montmorillonite on the solubility of whey protein isolate films in food model systems with different compositions and pH," *Food Hydrocolloids*, vol. 43, pp. 612–621, 2015.

[44] J. Pelleg, *Mechanical Properties of Materials*, Springer, 2012.

[45] T. D. Fornes and D. R. Paul, "Modeling properties of nylon 6/clay nanocomposites using composite theories," *Polymer*, vol. 44, no. 17, pp. 4993–5013, 2003.

[46] B. Chen and J. R. G. Evans, "Elastic moduli of clay platelets," *Scripta Materialia*, vol. 54, no. 9, pp. 1581–1585, 2006.

[47] A. B. Morgan, "Flame retarded polymer layered silicate nanocomposites: a review of commercial and open literature systems," *Polymers for Advanced Technologies*, vol. 17, no. 4, pp. 206–217, 2006.

[48] V. Molajavadi and H. Garmabi, "Predicting the youngs modulus of intercalated and exfoliated polymer/clay nanocomposites," *e-Polymers*, vol. 11, p. 219, 2011.

[49] O. Weizman, A. Dotan, Y. Nir, and A. Ophir, "Modified whey protein coatings for improved gas barrier properties of biodegradable films," *Polymers for Advanced Technologies*, vol. 28, no. 2, pp. 261–270, 2016.

[50] M. Schmid, W. Zillinger, K. Müller, and S. Sängerlaub, "Permeation of water vapour, nitrogen, oxygen and carbon dioxide through whey protein isolate based films and coatings-Permselectivity and activation energy," *Food Packaging and Shelf Life*, vol. 6, pp. 21–29, 2015.

[51] W. J. Choi, H.-J. Kim, K. H. Yoon, O. H. Kwon, and C. I. Hwang, "Preparation and barrier property of poly(ethylene terephthalate)/clay nanocomposite using clay-supported catalyst," *Journal of Applied Polymer Science*, vol. 100, no. 6, pp. 4875–4879, 2006.